Propagation of phase nonanalytical points in fast- and slow-light media

Yuma Morita and Makoto Tomita
Department of Physics, Faculty of Science, Shizuoka University, 836, Ohya, Suruga-ku, Shizuoka, 422-8529, Japan
(Received 11 May 2017; published 7 August 2017)

We performed a series of experiments to examine the arrival of phase nonanalytical points in fast- and slow-light media, using a Gaussian-shaped temporal pulse and encoding phase nonanalytical points at various positions within the pulse envelope. For the phase nonanalytical points, the amplitude of the slowly varying pulse envelope, as well as any order of the derivatives, is continuous, but the phase of the carrier wave is discontinuous. The phase nonanalytical points were neither advanced nor delayed, but appeared at the same instance as they entered the fast- and slow-light media, in good accordance with the idea that the information velocity was equal to the velocity of light in a vacuum, c, or in the background medium.

DOI: 10.1103/PhysRevA.96.023813

I. INTRODUCTION

Electromagnetic waves, including radio waves, microwaves, and light, may be the most popular medium for the conveyance of information. Several methods are employed for encoding signals using electromagnetic waves. Amplitude modulation (AM) is a method where the amplitude of the carrier wave is modulated by the signal, while the phase of the carrier wave is kept constant. In the frequency modulation (FM) scheme, the amplitude is kept constant and the signal is transmitted through varying the carrier frequency, which is dependent on the phase of the carrier waves. Different methods have both advantages and disadvantages. For example, FM is less prone to interference, and as such less susceptible to noise as amplitude fluctuations during the interference process can be compensated for. In addition, FM has much better sound quality due to the wider bandwidth. In contrast, AM occupies a narrow bandwidth, and therefore more communication channels are available within the same frequency region.

The problem of information that can be encoded on electromagnetic waves has long been debated, especially in a fast-light system. In an anomalous dispersive region, the smooth peak of a Gaussian-shaped pulse travels at a speed predicted by the conventional definition of group velocity, even in superluminal propagation, provided the propagation distance is sufficiently short [1–6]. Although the superluminal pulse velocity seemingly contradicts Einstein's special relativity, it is well understood that the arrival of the pulse peak or even the main body of the smooth superluminal pulse can be predicted using a Taylor expansion of the leading part of the pulse; thus the superluminal pulse peak has no new information. It is proposed that the true information is not contained in the pulse peak, but instead is carried by the nonanalytical points or singularities along the wave packets [7–12]. The pulse front edge is one of the nonanalytical points. Sommerfeld and Brillouin analyzed the propagation of square-modulated pulses through a broad-bandwidth Lorentz medium under far off-resonance conditions [1]. They determined that the front of the precursor always travels at the velocity of light, c.

Many discussions have been developed around practical nonanalytical points because there are crucial gaps between ideal (or mathematical) nonanalytical points and practical (or physical) nonanalytical points. One of the significant differences is the effect of fluctuations and noise [13–15]. The velocity of detectable information in superluminal media has been investigated using the bit error rate as a basis. The effect on the relative strength of the detector noise with respect to the medium noise and the effect of the propagation distance were studied. To increase the signal-to-noise ratio at the output position, more signal is required to arrive, resulting in retardation of the signal. Another issue may be the effect of the bandwidth [16,17]. An ideal nonanalytical point localizes at an infinitesimal time point and thus it requires an infinite spectral bandwidth and energy. In contrast, the bandwidth of any practical nonanalytical point is restricted to finite values; therefore, the practical nonanalytical point acquires analyticity and delocalizes, spreading across a region of time.

Our interest here lies in another question, that is, whether a phase nonanalytical point could have the nature of the true signal as with an amplitude nonanalytical point, and how the nonanalytical point could propagate through a fast medium. For phase nonanalytical points, the amplitude, as well as any order of the derivatives, is continuous, but the phase of the carrier wave is discontinuous. The propagation of a nonanalytic step-phase-modulated light pulse has been studied in stacking optical precursors [18]. So far, most experiments on nonanalytical points have, however, been performed using amplitude- or intensity-modulated pulses, including the front edge of a Gaussian pulse [7–17,19–22]. We performed a series of experiments to examine the arrival of phase nonanalytical points in fast- and slow-light media, using a Gaussian-shaped temporal pulse as the input pulse and encoding phase nonanalytical points at various positions within the pulse envelope. Experimental results showed good agreement with the idea that a phase nonanalytical point behaves as information and that the propagation velocity is equal to the velocity of light in a vacuum or in the background medium, independent of the group velocity and, thus, the phase nonanalytical points can also be interpreted as the signal. We examined the propagation of phase nonanalytical points because information velocity is an important concept in physics, and preserves fundamental relativistic causality.

II. EXPERIMENTS

Our experimental setup is illustrated schematically in Fig. 1. We used fiber ring resonators, which offer highly controllable

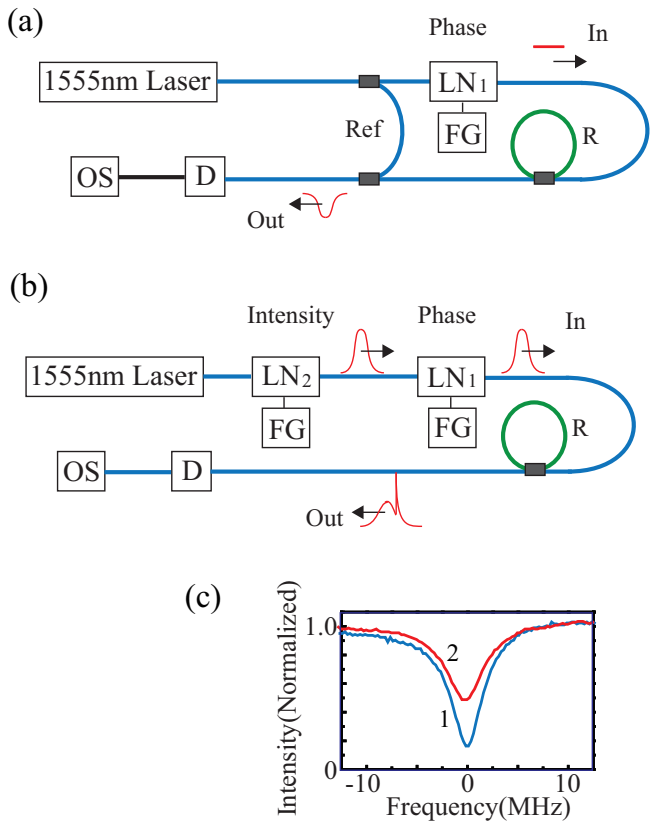

FIG. 1. Schematic illustration of the experimental setup; (a) for the purely phase-modulated beam propagation, and (b) for the Gaussian-shaped pulse propagation with the phase nonanalytical point. LN_1 and LN_2: $LiNbO_3$ modulators; D: detector; FG: function generator; OS: oscilloscope; Ref: reference beam. The green circle represents the ring resonator. (c) The transmission spectra as a function of detuning frequency. The blue and red lines (denoted lines 1 and 2, respectively) are for the undercoupling and overcoupling ring resonators, respectively. For the measurements of the transmission spectra, LN modulators were used in open mode.

dispersions via the cavity loss, x, and coupling strength, y, between the fiber and the ring resonator. Our interest here lies in the propagation of phase nonanalytical points and not in the dispersion characteristics of the ring resonators, which have already been studied in detail [23,24]. The stationary input-output characteristics of the resonator can be analyzed using directional coupling theory. The output light intensity, $T(\nu)$, as a function of incident laser frequency, ν, shows a periodic dip structure due to the resonance. The dispersion relationship depends on the loss and coupling strength. For the undercoupling condition ($x < y$), the transmission phase $\theta(\nu)$ shows anomalous dispersion at the center of the resonances. The group delay is expected to be negative, $\tau_g = \partial\theta/\partial\omega < 0$, corresponding to superluminal pulse propagation, namely, fast light. In contrast, for the overcoupling condition ($x > y$), the transmission phase shows normal dispersion, and one would expect slow light.

In the current study, 90:10 and 80:20 couplers were used to achieve undercoupling and overcoupling conditions, respectively. We inserted additional loss elements within the ring resonator to control the loss parameter. The physical length of the ring, L_R, was 2.0 m. Figure 1(c) shows examples of a transmission spectra as a function of detuning frequency. The blue and red lines represent the resonance spectra of the ring resonator in undercoupling and overcoupling conditions, respectively. The resonance widths, $\delta\nu_R$, were 3.4 and 4.5 MHz, respectively. An Er-fiber laser was used as the incident light source. The spectral width was 1 kHz, and the laser frequency was tuned by piezoelectric control of the cavity length. Figure 1(a) shows the setup for the experiments on the propagation of purely phase-modulated beams using a phase-sensitive homodyne detection method. The light beam from the Er-fiber laser was split into two beams. One beam passed through a $LiNbO_3$ modulator (LN_1), which modulated the phase, and then propagated through the ring resonator. The other beam from the Er-fiber laser was used as a reference. The signal beam that passed through the ring resonator was coupled to the reference beam. The intensity was detected by an InGaAs photodetector and reordered using a 600-MHz digital oscilloscope. Figure 1(b) shows a different setup for the experiments on the propagation of a Gaussian-shaped pulse with a phase nonanalytical point. The incident beam passed two serially configured modulators. The modulator LN_2 modulated the intensity profile and LN_1 modulated the phase independently. The transmitted pulses were detected using intensity without using a reference beam.

Before proceeding with experiments on the nonanalytical points, we first examined the propagation of a purely phase-modulated continuous beam through the ring resonator. For this purpose, we prepared input light beams as

$$E_{\text{in}}(t) = A\exp\{-i[\omega t + \varphi(t)]\},$$

where

$$\varphi(t) = \varphi_{\text{ph}}\exp\left[-\left(\frac{t}{t_{\text{ph}}}\right)^2\right]. \quad (1)$$

φ_{ph} represents the depth of phase modulation, t_{ph} is the temporal width of the Gaussian phase modulation, and A is a constant. Figure 2(a) shows the input light intensity observed without the reference beam. As the amplitude of the input beam represented by Eq. (1) was constant, the intensity appeared completely flat as a function of time. Figures 2(b)–2(d) show the transmitted light intensity through the undercoupling ring resonator, that is, the fast-light medium. When the temporal width of the modulation was short compared with the inverse of the resonance width, $t_{\text{ph}} < {\delta\nu_R}^{-1}$, the output beam intensity showed waving patterns. These structures could be attributed to the higher-order dispersion effects, $\partial^2\theta/\partial\omega^2$ in the ring resonator. As t_{ph} was increased, the waving patterns became weak and the transmitted temporal profile became a flat line, indicating that the phase-modulated output light beam could not be detected on an intensity basis.

For the detection of the phase-modulated output pulse, we introduced a reference beam as

$$E_{\text{ref}}(t) = B\exp[-i(\omega t + \varphi_{\text{ref}})], \quad (2)$$

where B is a constant. The output pulses were observed in the homodyne detection method using the setup shown in Fig. 1(a). Figure 3 shows the output beam in fast-light medium observed using the same input beam that was used in Fig. 2. The top and second rows are input and output (on-resonance condition;

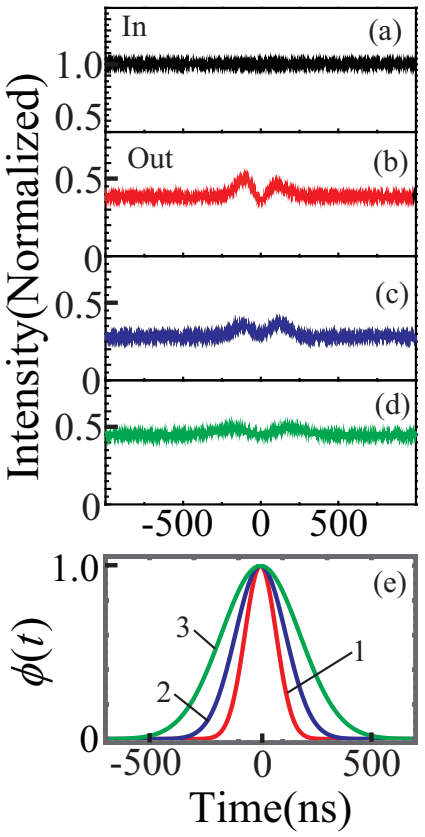

FIG. 2. (a) The black line represents experimental observation of input light of a purely phase-modulated continuous beam in the intensity basis. (b)–(d) represent experimental observations of output light of the purely phase-modulated beam in the intensity basis. The temporal durations were t_p = (b) 170, (c) 270, and (d) 420 ns. (e) Red (denoted line 1), blue (line 2), and green (line 3) lines represent the Gaussian-shaped phase modulation used in experiments shown in (b)–(d), respectively.

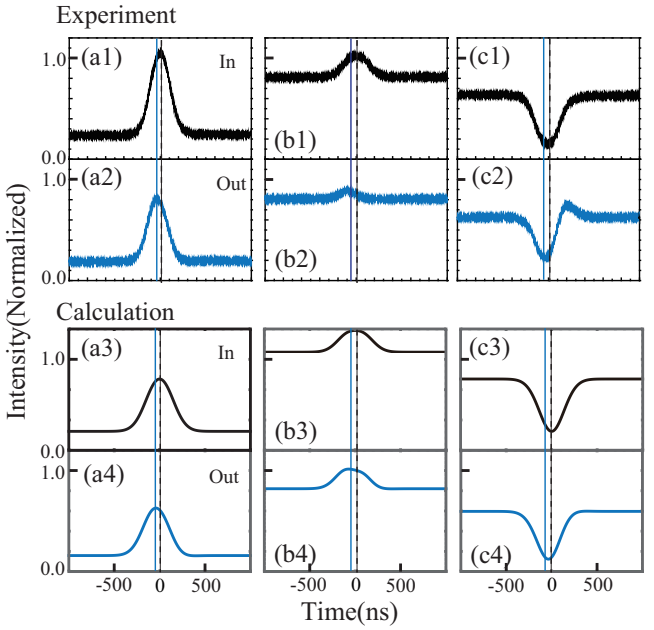

FIG. 3. The black lines in the top row [(a1), (b1), and (c1)] and the blue lines in the second row [(a2), (b2), and (c2)] are experimental observations of input and output temporal profiles, respectively, detected by the phase-sensitive homodyne method in the fast-light system. The input beam was a continuous light beam with the Gaussian-shaped phase modulation based on Eq. (1). The reference phases were $\varphi_{\rm ref}$ = (a) 0.9π, (b) 0.4π, and (c) -0.6π. The third row [(a3), (b3), and (c3)] and the bottom row [(a4), (b4), and (c4)] are calculated curves for the input (black lines) and output (blue lines) temporal profiles corresponding to the experiments in the top and second rows in the same columns, respectively. The heights of input and output pulses were normalized. The vertical dashed black lines represent the peak time of the input pulses ($t = 0$) and the vertical solid blue lines represent the peak time of the output pulses.

blue lines) temporal profiles, respectively. The reference phases, $\varphi_{\rm ref}$, were (a) 0.9π, (b) 0.4π, and (c) -0.6π rad. The Gaussian-shaped profiles appeared in the homodyne detection method and the pulse peak was advanced, with $\tau_{\rm ph} = -41$ ns ($\varphi_{\rm ref} = 0.9\pi$ rad), which showed good agreement with the calculated group delay of $\tau_g = -39$ ns. Although the ratio of signal height to the baseline was dependent on $\varphi_{\rm ref}$, the advancement of the Gaussian peak was almost consistent between the cases. The lower two rows are calculated curves for the input and output pulse profiles, respectively, corresponding to the experiments in Figs. 3(a)–3(c). The calculation shows good agreement with the experiments.

We repeated similar experiments in a slow-light medium using the overcoupling ring resonator. Figure 4 shows similar experimental results. The top and second rows are input (black lines) and output (red lines) temporal pulse profiles, respectively, for three reference phases. The Gaussian pulse peak was delayed by $\tau_{\rm ph} = 84$ ns ($\varphi_{\rm ref} = -0.6\pi$ rad), which shows good agreement with the calculated group delay. So far, most experiments on fast and slow light have been performed using intensity-modulated pulses. The results shown in Figs. 3 and 4 confirmed experimentally that the Gaussian-shaped phase modulation propagates with the relevant group velocity in the fast- and slow-light media.

We next examined the propagation of phase nonanalytical points using the setup shown in Fig. 1(b). For this purpose, we prepared a Gaussian-shaped intensity profile and encoded a phase nonanalytical point at various positions within the pulse envelope as

$$E_{\rm in}(t) = C \exp\left\{-\left(\frac{t}{t_a}\right)^2 - i[\omega t + \varphi(t)]\right\},$$

with

$$\varphi(t) = \varphi_{\rm NA}\Theta(t_{\rm NA}) = \begin{cases} 0 & t < t_{\rm NA} \\ \varphi_{\rm NA} & t \geqslant t_{\rm NA} \end{cases}, \qquad (3)$$

where $\Theta(t)$ is a Heaviside function and C is a constant. In experiments, the intensity of the incident laser beam was modulated to have a Gaussian-shaped pulse profile with a temporal duration of t_a using $\rm LN_2$. Then, the phase nonanalytical point was encoded at a time of $t_{\rm NA}$ using $\rm LN_1$. The transmitted pulses were detected in an intensity basis without the reference beam. Figure 5 shows the output pulse intensity through the fast-light medium, that is, the undercoupling ring resonator. The encoding time, $t_{\rm NA}$, was 30 ns. In Fig. 5(a), the modulation depth,

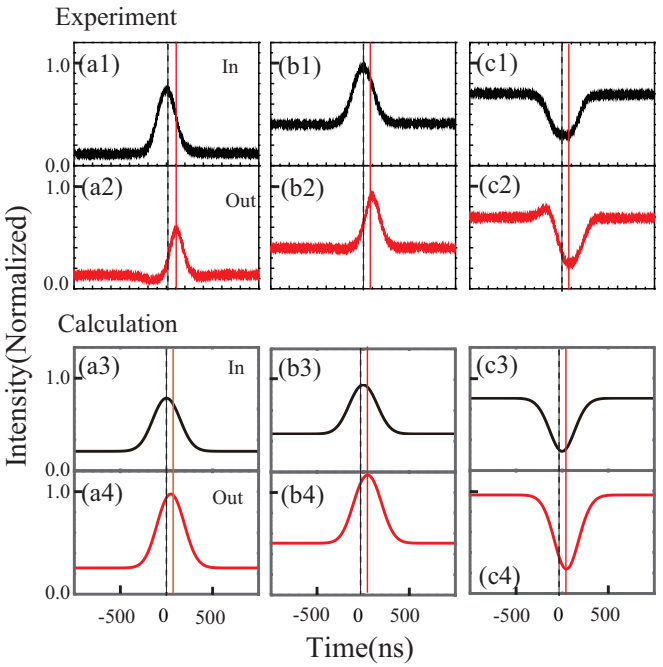

FIG. 4. Plots similar to Fig. 3 in the slow-light system. The black lines in the top row [(a1), (b1), and (c1)] and the red lines in the second row [(a2), (b2), and (c2)] are experimental observations of the input and output temporal profiles, respectively, detected by the homodyne method. The reference phase was $\varphi_{\mathrm{ref}} =$ (a) -1.1π, (b) -1.2π, and (c) -0.6π rad. The third row [(a3), (b3), and (c3)] and bottom row [(a4), (b4), and (c4)] are calculated curves for the input (black lines) and output (red lines) temporal pulse profiles corresponding to the experiments in the top and second rows in the same columns, respectively. The vertical dashed black lines represent the peak time of the input pulses ($t = 0$) and the vertical solid red lines represent the peak time of the output pulses.

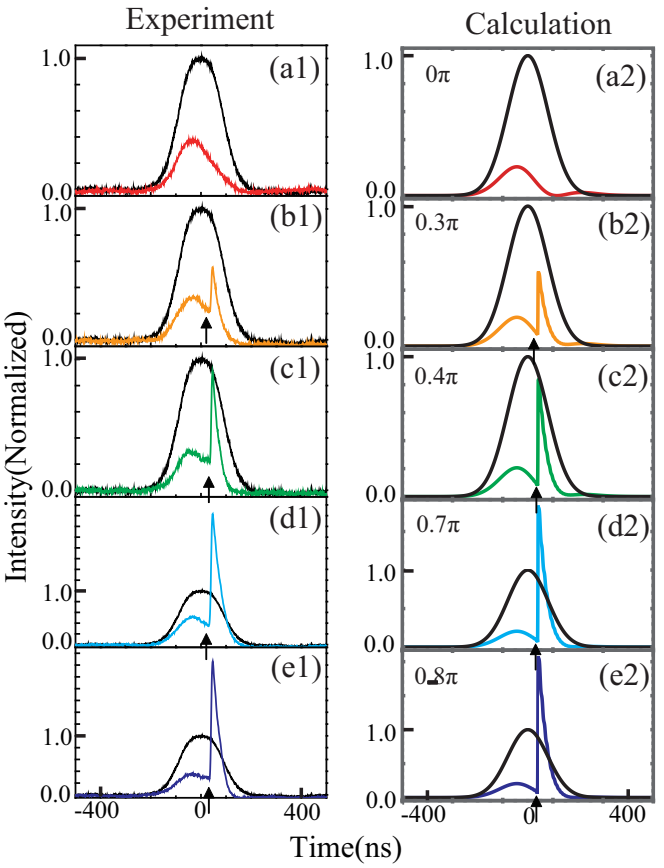

FIG. 5. The black lines represent input pulses with the Gaussian-shaped intensity profile on which the phase nonanalytical point was encoded, based on Eq. (3), for different modulation depths. The colored lines are output temporal profiles through the fast-light medium. The modulation depth was $\varphi_{\mathrm{NA}} =$ (a) 0, (b) 0.3π, (c) 0.4π, (d) 0.7π, and (e) 0.8π rad. The encoding time was $t_{\mathrm{NA}} = 30$ ns and is indicated with the upward black arrows. The pulse heights were normalized by the height of the input pulse. The left and right columns are experimental observations and numerical calculations, respectively. Note that the vertical scales in (d,e) are reduced.

φ_{NA}, was 0 rad; hence the input pulse was a smooth Gaussian pulse without the nonanalytical point. The output pulse peak was advanced by $\tau_{\mathrm{am}} = -41$ ns, which shows good agreement with the observed value in the phase-modulated beam of $\tau_{\mathrm{ph}} = -41$ ns. In Fig. 5(b), the modulation depth increased as $\varphi_{\mathrm{NA}} = 0.3\pi$ rad. When the phase nonanalytical point was introduced, a sharp spike appeared at $t_K = 30$ ns. This spike could be attributed to the resonance precursor [19–22].

A nonanalytical point can be represented by a relatively broad feature in the frequency domain, to which the medium cannot respond. Therefore, nonanalytical points are always associated with optical precursors. Sommerfeld and Brillouin first analyzed the propagation of an amplitude-modulated step pulse, assuming broadband and off-resonance conditions. Under these conditions, precursors are negligible; however, the amplitude of the precursor may be large under resonant conditions [19–22]. In the present case, the large observed transient spike could be described by superposition of a postcursor generated by the trailing edge of the pulse section prior to t_{NA}, with a precursor generated by the leading edge of the pulse section following t_{NA}. The phase of the former and latter sections of the pulse are related to the phases $\varphi = 0$ and $\varphi = \varphi_{\mathrm{NA}}$, respectively. Further, as the postcursor predominantly consists of the electric field components that circulate within the ring resonator, whereas the precursor consists of direct components that bypass the ring, the postcursor is phase shifted by π radians relative to the precursor [24].

Taking these facts into account, we examined the effect of the modulation depth φ_{NA} on the height of the transient spike. Figures 5(c)–5(e) show the intensity of the output pulse for larger modulation depths φ_{NA} at encoding time $t_{\mathrm{NA}} =$ 30 ns. When $\varphi_{\mathrm{NA}} = 0$, the postcursor and precursor summed destructively, hence no spike was observed. This corresponds to a situation whereby the pulse has no nonanalytical point [see Fig. 5(a)]. As φ_{NA} increased, the height of the spike increased. This is because the postcursor and precursor interfere constructively. The height exhibited a maximum around $\varphi_{\mathrm{NA}} = \pi$ rad as φ_{NA} canceled the π phase shift between the postcursor and precursor. Figure 6 summarizes the height of the spike at the kick position in the output pulse as a function of modulation depth φ_{NA}.

Figure 7 shows the output pulse through the fast-light medium for Gaussian-shaped pulses encoded with a phase

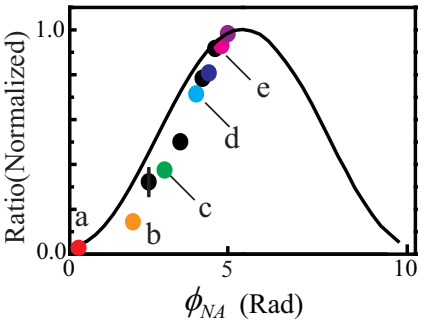

FIG. 6. The height of the transient spike at the kick position t_K in the output pulse as a function of the modulation depth φ_{NA}. The colored solid circles indicated by a–e correspond to the experimental results shown in Figs. 5(a)–5(e), respectively. The black solid circles (unlabeled) represent other results not shown in Fig. 5. The solid line represents the corresponding simulations.

nonanalytical point at different encoding times, t_{NA}. The modulation depth was constant, $\varphi_{\mathrm{NA}} = 0.6\pi$ rad. Figure 8 summarizes the peak position, τ_{am}, and kick positions, t_K, observed in the output pulse as a function of the encoding time, t_{NA}. Although the pulse peak was advanced and independent of the encoding time, the kick positions of the transient spike, t_K, followed the encoding time t_{NA}. The nonanalytical points were neither advanced nor delayed, but appeared at the same instance as they entered the ring resonator.

We performed similar experiments in the slow-light system using the overcoupling ring resonator. Figure 9 shows experimental results of the output pulse profiles. In Fig. 9(a), the modulation depth was $\varphi_{\mathrm{NA}} = 0$ rad, and hence the input pulse was a smooth Gaussian pulse without the nonanalytical point. The output pulse peak was delayed by 83 ns, which shows good agreement with the observed value in the phase-modulated beam. In Figs. 9(b)–9(d) $\varphi_{\mathrm{NA}} = 0.6\pi$ rad and t_{NA} was changed. Although the pulse peak position was delayed, the arrivals of the phase nonanalytical points indicated by the transient spike were neither advanced nor delayed, but appeared at the same instance as they entered the medium. The kick positions of the transient spike, t_K, followed the encoding time, t_{NA}. These experimental results in slow-light media are also in good accordance with the idea that the phase nonanalytical point acts as a signal and the relevant information velocity is equal to the velocity of light in a vacuum or the background medium even in the slow-light media.

III. DISCUSSION

A. Lorentz medium

The phase nonanalytical points were neither advanced nor delayed; rather, they appeared at the same instance as they entered the ring resonators. This behaviour may be a universal characteristic in causal dispersive systems. To investigate this universality, we calculated the propagation of phase nonanalytical points through a Lorentz medium. The spectral form was assumed to be $g(\nu) = \beta/[(\nu_0 - \nu) - i\gamma]$, where ν_0 is the resonant frequency and β is a constant describing the light-matter interaction. Anomalous dispersion was observed at the resonance frequency $\nu = \nu_0$.

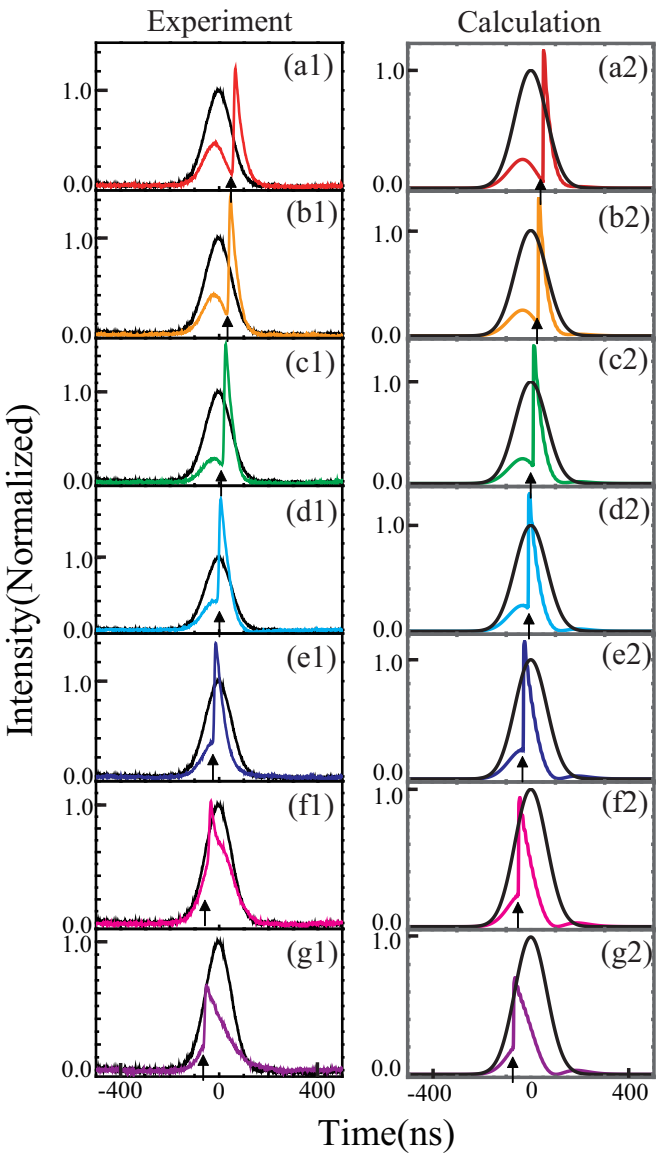

FIG. 7. The black lines represent input pulses with Gaussian-shaped intensity profile on which the phase nonanalytical point was encoded based on Eq. (3), at different encoding times. The colored lines are output temporal pulse profiles through the fast-light medium. The encoding times were t_{NA} = (a) 50, (b) 30, (c) 10, (d) −10, (e) −30, (f) −50, and (g) −70 ns, which are indicated with the upward black arrows. The modulation depth was $\varphi_{\mathrm{NA}} = 0.6\pi$ rad. The left and right columns are experimental observations and numerical calculations, respectively.

Figure 10 shows input and output pulse profiles. The input pulse was a Gaussian intensity profile with a phase nonanalytical point at $t_{\mathrm{NA}} = 50$ ns. As with an undercoupling ring resonator, although the pulse peak advanced, reflecting the anomalous dispersion at the center of the Lorentz line, the arrival time of the phase nonanalytical points indicated by the transient spike was neither advanced nor delayed, appearing at the same instance as they entered the Lorentz medium. These simulated data suggest that propagation of the phase nonanalytical point is an intrinsic feature of causal dispersive systems.

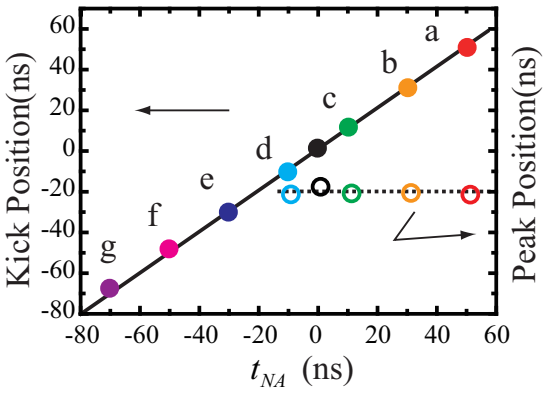

FIG. 8. Peak positions τ_{am} and kick positions t_K in the output pulse as a function of the encoding time of the phase nonanalytical point, t_{NA}. The open and solid circles represent the experimentally observed peak and kick positions, respectively. The colored solid circles indicated by a–g represent the experimental results shown in Figs. 7(a)–7(g), respectively. The black solid circle (unlabeled) represents the result not shown in Fig. 7.

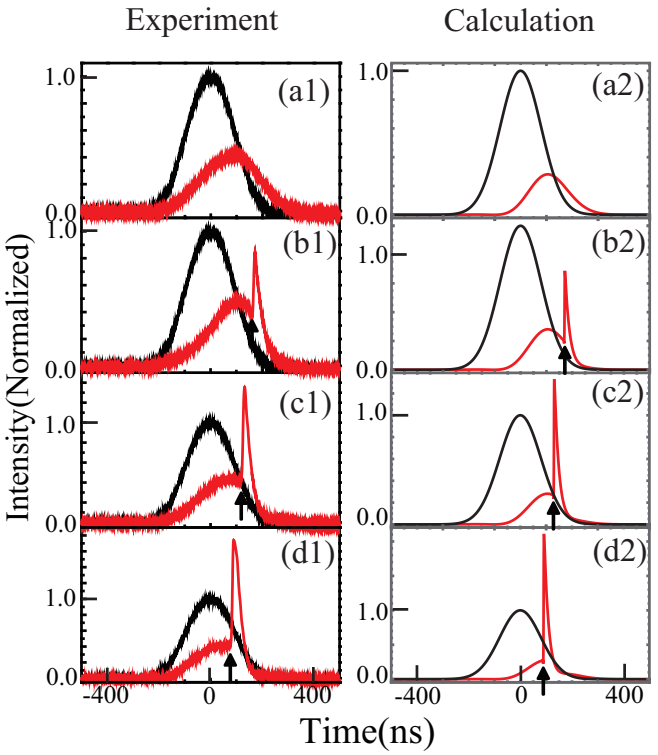

FIG. 9. The black lines represent the input pulses with Gaussian-shaped intensity profile, on which the phase nonanalytical point was encoded based on Eq. (3). The red lines represent output pulses through the overcoupling ring resonator. (a) The modulation depth was $\varphi_{\mathrm{NA}} = 0$ rad; hence the input pulse was a smooth Gaussian pulse without the nonanalytical point. (b)–(d) $\varphi_{\mathrm{NA}} = 0.6\pi$ rad and the encoding times were $t_{\mathrm{NA}} = 170$, 130, and 90 ns, respectively. The left and right columns are experimental observations and numerical calculations, respectively.

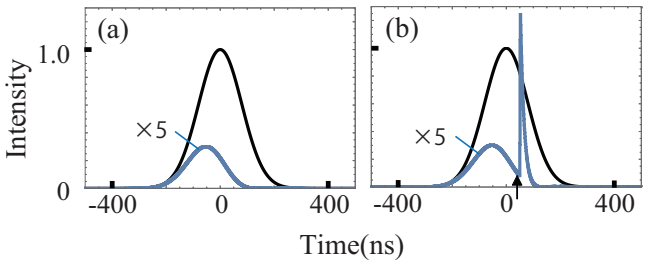

FIG. 10. The black lines show the input pulse with a Gaussian intensity profile, on which the phase nonanalytical point was encoded based on Eq. (3). The modulation depth was (a) $\varphi_{\mathrm{NA}} =$ (a) 0 and (b) 0.2π rad. The blue lines show calculated output pulse profiles through a Lorentzian absorption medium with $\nu_0 = 2.0 \times 10^{14}$ Hz, $\beta = 5.0 \times 10^2$ Hz, and $\gamma = 3.0 \times 10^6$ Hz, over a propagation distance $z = 0.005$ m.

B. Phase nonanalytical point in slowly varying envelope

An ideal nonanalytical point localizes at an infinitesimal time point and thus requires infinite spectral bandwidth. In contrast, the bandwidth of any practical nonanalytical point is restricted to a finite value; therefore, the nonanalytical point delocalizes and acquires analyticity. It was discussed that the practical nonanalytical point neither disconnects nor connects completely to the neighboring regions in the pulse and that the expansion of the leading part of the pulse can predict the forthcoming pulse shape beyond practical nonanalytical points [16].

From the point of view of a phase nonanalytical point, a true phase nonanalytical point should change the phase within one optical cycle, namely, in a femtosecond time scale. For the discussion of the present nonanalytical points, it is convenient to introduce the slowly varying envelope as $E_{\mathrm{in}}(t) = \tilde{E}_{\mathrm{in}}(t)e^{-i\omega t}$ and $\tilde{E}_{\mathrm{in}}(t) = |\tilde{E}_{\mathrm{in}}(t)|e^{-i\tilde{\varphi}_{\mathrm{in}}}$. In addition, for the phase nonanalytical points,

$$\lim_{\varepsilon\to 0}|\tilde{E}_{\mathrm{in}}(t_{\mathrm{NA}}-\varepsilon)| = \lim_{\varepsilon\to 0}|\tilde{E}_{\mathrm{in}}(t_{\mathrm{NA}}+\varepsilon)|,$$
$$\lim_{\varepsilon\to 0}\tilde{\varphi}_{\mathrm{in}}(t_{\mathrm{NA}}-\varepsilon) \neq \lim_{\varepsilon\to 0}\tilde{\varphi}_{\mathrm{in}}(t_{\mathrm{NA}}+\varepsilon). \tag{4}$$

In our experiments, the bandwidth of the incident beam with the phase nonanalytical point was 400 MHz. In contrast, the bandwidth of the resonance of the present ring resonator was 3.4 MHz. Therefore, phase structures that have higher Fourier components than 3.4 MHz could be recognized as nonanalytical for the present ring resonator. For pulse propagation in dispersive media, a convenient analytic form to represent the outgoing pulses within the group-velocity approximation is given by Ref. [25] as

$$E(t,z) = \frac{1}{2\pi}e^{i(kz-\omega t)}\exp\left[z\left(\frac{1}{c}-\frac{1}{v_g}\right)\frac{\partial}{\partial t}\right]\tilde{E}_{\mathrm{in}}\left(t-\frac{z}{c}\right). \tag{5}$$

Equation (5) states that the electric field that propagated with superluminal $v_g > c$ over a distance z corresponds to an analytic continuation over time, $z/c - z/v_g > 0$, of $\tilde{E}_{\mathrm{in}}(t - z/c)$. We consider a pulse that propagates a distance z through a dispersive medium, and consider the electric fields in the pulse at times just before and after $t = z/c + t_{\mathrm{NA}}$, i.e., $E(t_{\mathrm{NA}} + z/c - \varepsilon, z)$ and $E(t_{\mathrm{NA}} + z/c + \varepsilon, z)$. Note that $t = z/c + t_{\mathrm{NA}}$ is the time when the nonanalytical point would

arrive if that pulse were to propagate in a vacuum for distance z. Using Eq. (5), these two electric fields are connected to $\tilde{E}_{\rm in}(t_{\rm NA}-\varepsilon)$ and $\tilde{E}_{\rm in}(t_{\rm NA}+\varepsilon)$, respectively. From Eq. (4), for phase nonanalytical points we may conclude that

$$\lim_{\varepsilon\to 0} E(t_{\rm NA}+z/c-\varepsilon,z) \neq \lim_{\varepsilon\to 0} E(t_{\rm NA}+z/c+\varepsilon,z). \quad (6)$$

Hence, the nonanalytical phase points propagate with velocity c rather than v_g.

IV. SUMMARY

In summary, we performed a series of experiments to examine the arrival of phase nonanalytical points in fast- and slow-light media, using a Gaussian-shaped temporal wave packet as the input pulse and encoding phase nonanalytical points at various positions. The phase nonanalytical points were neither advanced nor delayed, but appeared at the same instance as they entered the system. Similar behavior was observed for Lorentzian absorption lines. This indicates that the phase nonanalytical point may be the "true signal" in causal dispersive media, and that the information velocity is equal to the velocity of light in a vacuum (or the background media), in accordance with the causal principles observed in fast-light systems.

ACKNOWLEDGMENT

This work was supported by Japan Society for the Promotion of Science KAKENHI Grant No. 26287091.

[1] L. Brillouin, *Wave Propagation and Group Velocity* (Academic Press, New York, 1960).
[2] P. W. Milonni, *Fast Light, Slow Light and Left-Handed Light* (Taylor & Francis, New York, 2004).
[3] S. Chu and S. Wong, Linear Pulse Propagation in an Absorbing Medium, Phys. Rev. Lett. **48**, 738 (1982).
[4] L. J. Wang, A. Kuzmich, and A. Dogariu, Gain-assisted superluminal light propagation, Nature **406**, 277 (2000).
[5] A. I. Talukder, Y. Amagishi, and M. Tomita, Superluminal to Subluminal Transition in the Pulse Propagation in a Resonantly Absorbing Medium, Phys. Rev. Lett. **86**, 3546 (2001).
[6] G. M. Gehring, A. Schweinsberg, C. Barsi, N. Kostinski, and R. W. Boyd, Observation of backward pulse propagation through a medium with a negative group velocity, Science **312**, 895 (2006).
[7] R.Y. Chiao and A. M. Steinberg, Tunneling times and superluminality, in *Progress in Optics XXXVII*, edited by E. Wolf (Elsevier, Amsterdam, 1997), p. 345.
[8] M. D. Stenner, D. J. Gauthier, and M. A. Neifeld, The speed of information in a 'fast-light' optical medium, Nature (London) **425**, 695 (2003).
[9] M. D. Stenner, D. J. Gauthier, and M. A. Neifeld, Fast Causal Information Transmission in a Medium with a Slow Group Velocity, Phys. Rev. Lett. **94**, 053902 (2005).
[10] M. Tomita, H. Amano, S. Masegi, and A. I. Talukder, Direct Observation of a Pulse Peak Using a Peak-Removed Gaussian Optical Pulse in a Superluminal Medium, Phys. Rev. Lett. **112**, 093903 (2014).
[11] N. Brunner, V. Scarani, M. Wegmüller, M. Legré, and N. Gisin, Direct Measurement of Superluminal Group Velocity and Signal Velocity in an Optical Fiber, Phys. Rev. Lett. **93**, 203902 (2004).
[12] M. Tomita, H. Uesugi, P. Sultana, and T. Oishi, Causal information velocity in fast and slow pulse propagation in an optical ring resonator, Phys. Rev. A **84**, 043843 (2011).
[13] A. Kuzmich, A. Dogariu, L. J. Wang, P. W. Milonni, and R. Y. Chiao, Signal Velocity, Causality, and Quantum Noise in Superluminal Light Pulse Propagation, Phys. Rev. Lett. **86**, 3925 (2001).
[14] U. Vogl, R. T. Glasser, and P. D. Lett, Advanced detection of information in optical pulses with negative group velocity, Phys. Rev. A **86**, 031806(R) (2012).
[15] A. H. Dorrah and M. Mojahedi, Velocity of detectable information in faster-than-light pulses, Phys. Rev. A **90**, 033822 (2014).
[16] H. Amano and M. Tomita, Influence of finite bandwidth on the propagation of information in fast- and slow-light media, Phys. Rev. A **93**, 063854 (2016).
[17] H. Amano and M. Tomita, Luminal pulse velocity in a superluminal medium, Phys. Rev. A **92**, 063837 (2015).
[18] J. F. Chen, H. Jeong, L. Feng, M. M. T. Loy, G. K. L. Wong, and S. Du, Stacked Optical Precursors from Amplitude and Phase Modulations, Phys. Rev. Lett. **104**, 223602 (2010).
[19] H. Jeong, A. M. C. Dawes, and D. J. Gauthier, Direct Observation of Optical Precursors in a Region of Anomalous Dispersion, Phys. Rev. Lett. **96**, 143901 (2006).
[20] H. Jeong and U. Österberg, Coherent transients: optical precursors and 0π pulses, J. Opt. Soc. Am. B **25**, B1 (2008).
[21] D. Wei, J. F. Chen, M. M. T. Loy, G. K. L. Wong, and S. Du, Optical Precursors with Electromagnetically Induced Transparency in Cold Atoms, Phys. Rev. Lett. **103**, 093602 (2009).
[22] T. Oishi, R. Suzuki, P. Sultana, and M. Tomita, Optical precursors in coupled-resonator-induced transparency, Opt. Lett. **37**, 2964 (2012).
[23] K. Totsuka, N. Kobayashi, and M. Tomita, Slow Light in Coupled-Resonator-Induced Transparency, Phys. Rev. Lett. **98**, 213904 (2007).
[24] K. Totsuka and M. Tomita, Slow and fast light in a microsphere–optical fiber system, J. Opt. Soc. Am. B **23**, 2194 (2006).
[25] G. Diener, Superluminal group velocities and information transfer, Phys. Lett. A **223**, 327 (1996).